

Review

Advances in Mid-IR Fiber Lasers: Tellurite, Fluoride and Chalcogenide

Mario Christian Falconi, Dario Laneve and Francesco Prudenzano *

Department of Electrical and Information Engineering, Politecnico di Bari, 70125 Bari, Italy; mariochristian.falconi@poliba.it (M.C.F.); dario.laneve@poliba.it (D.L.)

* Correspondence: francesco.prudenzano@poliba.it; Tel.: +39-080-596-3781

Academic Editor: Stephen C. Bondy

Received: 28 March 2017; Accepted: 13 June 2017; Published: 15 June 2017

Abstract: A review on the recent progress in modeling and fabrication of medium infrared (Mid-IR) fiber lasers is reported. The main objective is to illustrate some recent examples of continuous wave optical sources at wavelengths longer than those commonly employed in telecom applications and allowing high beam quality. A small number of Mid-IR lasers, among the large variety of schemes, glasses, dopants and pumping schemes reported in literature, is selected on the basis of their slope efficiency and threshold pump power. In particular, tellurite, fluoride and chalcogenide fiber lasers are considered. More details are given with reference to the novel pumping schemes.

Keywords: fiber optics; fiber lasers; advanced fiber materials

1. Introduction

Recent and impressive advances have been obtained in the field of medium infrared (Mid-IR) optical sources. Mid-IR fiber lasers constitute only a part of these devices and their actual interest is strictly related to the comparison of their performances with those of alternative solutions as quantum cascade lasers (QCLs) [1], optical parametric oscillators (OPOs) based on light-matter interaction in nonlinear propagation media [2], and frequency comb generation emitting a broad spectrum of discrete narrow lines [3]. In particular, QCLs have been recently exploited in a number of applications. Nowadays, these sources are available on the market at relatively low prices and exhibit, as their greatest strength, a wide tunability which allows a number of attractive applications requiring coherent light at both conventional and exotic wavelengths. Despite this panorama, fiber lasers remain key elements, since they have peculiar characteristics which make them unique optical sources. As an example, the beam quality achievable in Photonic Crystal Fiber (PCF) lasers cannot be obtained by means of QCLs. This advantage directly derives from the azimuthal symmetry of optical fibers generally lacking in planar/ridge waveguides. On the contrary, extremely complicated planar structures are required to obtain high beam quality emission in planar structures [4]. When beam quality, power scaling and narrow linewidth are required simultaneously, PCF based Mid-IR lasers are the most suitable solution. Short pulse generation and dispersion handling constitute further attractive characteristics of these optical sources. The possibility to vary the PCF microstructured cross-section is a well-known potential which can be exploited in the design in order to manage the modal group velocity dispersion (GVD) [5]. Therefore, Mid-IR fiber lasers cannot be substituted by other sources in some particular applications for which the aforesaid characteristics are required.

Mid-IR PCF lasers covering novel emission wavelengths can be considered solutions complementary to QCLs, OPOs and frequency comb generation [1–3,6]. They could be exploited in a huge quantity of potential applications, e.g., for active sensing in the field of medicine and environmental monitoring, coherent laser radar systems, laser imaging and remote chemical sensing [7–14]. Their exploitation in biological sensing is feasible since various water contaminants,

chemical substances, gases and biological molecules exhibit characteristic fingerprints in the medium infrared wavelength range (3–20 μm). They could find application in free space propagation systems since the earth atmosphere exhibits a number of Mid-IR transmission windows, e.g., in the 4.3–5.0 μm , 8–10 μm and 10–14 μm wavelength ranges. As a consequence, the optimization of Mid-IR PCF lasers allowing high brilliance and high beam quality could be a disruptive breakthrough for the operation principles and the equipment designed for remote sensing, aerospace, medical diagnosis and therapy, earth surface observation, monitoring of air contaminants or constituents such as CO_2 , and free space communication.

The research followed in order to construct Mid-IR PCF lasers is generally focused on three main topics: glass synthesis and optimization, optimal choice of dopants with reference to the used host glass, and more efficient pumping schemes. Among the glasses employed for the construction of Mid-IR PCF lasers, there are the fluoride, tellurite and chalcogenide ones. Typical rare earths employed for doping these glasses are erbium, ytterbium, praseodymium, dysprosium, thulium, terbium and holmium [8–11]. Cascade lasing and novel direct pumping schemes in active optical fibers, by means of QCLs, have been recently explored [10,11].

In this paper, a review on recent progress in modeling and fabrication of Mid-IR fiber lasers is reported. The depicted examples constitute a small number of Mid-IR lasers, among the large variety of schemes, glasses, dopants and pumping schemes described in literature. In particular, only tellurite, fluoride and chalcogenide fiber lasers are considered. A more detailed description is given with reference to the novel pumping schemes.

The review aims to give a panorama on those fiber lasers which emit beams at wavelengths beyond $\lambda = 1.55 \mu\text{m}$ and provide high beam quality M^2 compared to the other technical solutions which are available nowadays. Only continuous wave optical sources are taken into account.

Heterogeneous materials and technologies with different degrees of maturity are considered. The output power and the threshold pump power are important characteristics for fluoride or tellurite fiber lasers, but in several actual cases, a trade-off solution is searched for to obtain a feasible source. In low power niche applications, the minimization of threshold pump power can be considered the main objective.

The slope efficiency can be considered a parameter useful for comparison but a few considerations are required for a correct discussion. While tellurite and fluoride glasses are successfully employed for emission at wavelengths up to a few microns, chalcogenide glass seems more promising for longer wavelengths. They exhibit lower efficiency also due to a less mature technology. In fact, for chalcogenide lasers, the simple emission, even with low efficiency, constitutes an important result that could pave the way for fabrication of novel optical sources at longer wavelengths with higher beam quality. For all these reasons, the reported cases are not chosen with a completely homogeneous criterion. Moreover, the low number of reported examples cannot give an exhaustive view in the area of Mid-IR lasers, but only a partial idea on the state of the art.

2. Tellurite Glasses

Tellurite glass is largely employed in order to obtain Mid-IR fiber lasers. This kind of glass is transparent up to wavelengths of about 5 μm and exhibits a low phonon energy, close to 750 cm^{-1} , lower than that of silicate and germanate glasses. The hosted rare earths can exhibit high radiative rates and long lifetimes of the lasing levels [15–18]. The low phonon energy and the low background loss can enable a reduction of the laser threshold. Another important property of tellurite glass is the peculiar high solubility of rare earth ions within its amorphous matrix. The high rare earth concentrations allow the construction of very short fiber lasers, since the pump can be easily absorbed and the population inversion efficiently obtained. Moreover, this glass has a high refractive index. The strong confinement of light improves the light–matter interaction and increases the absorption and emission cross sections.

Tellurite glass technology can provide good laser efficiency. In [17], a Tm^{3+} -doped tellurite fiber was pumped with a diode-pumped $\text{Er}^{3+}/\text{Yb}^{3+}$ -doped silica fiber laser operating at the wavelengths

in the range from $\lambda = 1.57 \mu\text{m}$ to $\lambda = 1.61 \mu\text{m}$. A laser cavity providing emission in the range from $\lambda = 1.88 \mu\text{m}$ to $\lambda = 1.99 \mu\text{m}$ was obtained. The tellurite fiber had a core with 80TeO₂-10ZnO-10Na₂O mol.% composition and was doped with 1.0 wt.% Tm₂O₃ and 1.5 wt.% Yb₂O₃; the cladding had a 75TeO₂-15ZnO-10Na₂O mol.% composition. The core and the cladding diameters were $D_c = 13 \mu\text{m}$ and $D_{cl} = 125 \mu\text{m}$, respectively, the numerical aperture $NA = 0.29$, and the fiber was uncoated. The pump source was employed to excite the Tm³⁺ ions directly into the ³F₄ upper laser level. The CW output power was $P_s = 280 \text{ mW}$ with a very high slope efficiency of $\eta = 76\%$, for a fiber having length of $L = 32 \text{ cm}$, was demonstrated. This result was an apparent demonstration of the potential high efficiency lasing in tellurite fibers at wavelengths longer than $\lambda = 1.56 \mu\text{m}$.

Co-doping is a useful technique in order to increase the lasing efficiency. As an example, in [18], an efficient laser output at the wavelength $\lambda = 2.052 \mu\text{m}$ was obtained from a Nd³⁺/Ho³⁺ co-doped tungsten tellurite fiber laser. The tellurite fiber was fabricated by a suction technique with the core and cladding diameters $D_c = 32 \mu\text{m}$ and $D_{cl} = 125 \mu\text{m}$, respectively, the numerical aperture was $NA = 0.28$ and the fiber was $L = 5 \text{ cm}$ long. Figure 1 illustrates the emission spectra of Ho³⁺ and Nd³⁺/Ho³⁺ co-doped tungsten tellurite glasses. The improvement of the emission intensity by considering Nd³⁺/Ho³⁺ co-doping is apparent. The first dichroic mirror has a reflectivity of $R_1 = 99.7\%$ at the signal wavelength and it is highly transparent at the pump wavelength. The second dichroic mirror is partially reflective ($R_2 = 86.8\%$) at the signal wavelength and highly reflective ($R_2 = 89.7\%$) at the pump wavelength. Nd³⁺ and Ho³⁺ concentrations were both equal to $10^{20} \text{ ions/cm}^3$. A 795 nm laser diode was employed for the pumping. The large energy transfer coefficient from Nd³⁺ to Ho³⁺ and the high gain coefficient of Ho³⁺: ⁵I₇ → ⁵I₈ transition allowed to obtain an efficient emission at wavelength $\lambda = 2052 \text{ nm}$. This result was obtained even if the propagation loss was close to 4.44 dB/m at 1310 nm.

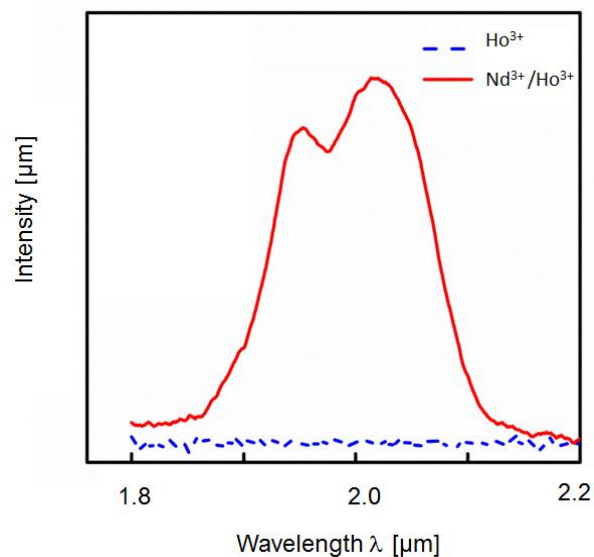


Figure 1. Emission spectra of Ho³⁺ and Nd³⁺/Ho³⁺ co-doped tungsten tellurite glasses. Figure adapted from [18].

Figure 2 illustrates the laser output power P_s versus the absorbed pump power P_p of the Nd³⁺/Ho³⁺ co-doped tungsten tellurite fiber laser of [18]. The maximum output power is $P_s = 12 \text{ mW}$ and the slope efficiency is $\eta = 11.2\%$. These values are not very interesting if compared to other lasers, but the power threshold is close to $P_{th} = 38 \text{ mW}$, which is very low with respect to that of Tm³⁺/Yb³⁺ doped tellurite fiber lasers with similar pumping scheme and fiber geometry. The aforesaid results indicate that the Nd³⁺/Ho³⁺ co-doped tungsten tellurite glass fiber can be considered a promising laser medium candidate for achieving ultra-compact and efficient lasers at wavelengths near $\lambda = 2 \mu\text{m}$.

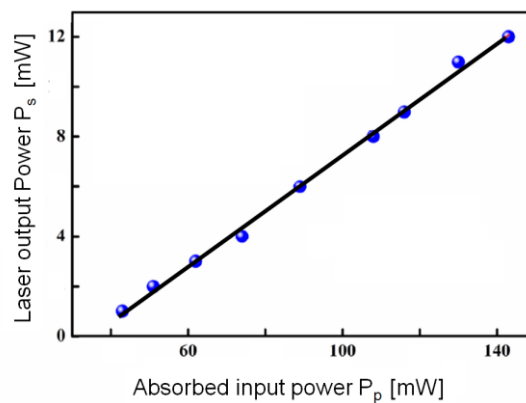


Figure 2. Characteristic of the $\text{Nd}^{3+}/\text{Ho}^{3+}$ co-doped tungsten tellurite fiber laser. The blue points are measured. Figure adapted from [18].

Co-doping technique as a successful strategy to improve the laser efficiency was utilized also in [19]. A single mode tellurite fiber was employed with an Er^{3+} ion core density of $0.9 \times 10^{20} \text{ cm}^{-3}$ and a Ce^{3+} ion core density of $2.1 \times 10^{20} \text{ cm}^{-3}$. Moreover, the fiber had numerical aperture $\text{NA} = 0.21$, core diameter $D_c = 4 \mu\text{m}$, length $L = 22 \text{ cm}$, mole percentage concentration of core $80\text{TeO}-10\text{ZnO}-10\text{Na}_2\text{O}$, mole percentage concentration of inner cladding $75\text{TeO}-15\text{ZnO}-10\text{Na}_2\text{O}$. The refractive index of the core and cladding were $n_c = 2.0448$ and $n_{cl} = 2.0224$ at the wavelength $\lambda = 633 \text{ nm}$, respectively, and the background loss of the fiber was 2 dB/cm at the wavelength $\lambda = 1.7 \mu\text{m}$. The forward pump and backward pump sources were provided from lasers at the wavelength $\lambda = 980 \text{ nm}$ and at the wavelength $\lambda = 1480 \text{ nm}$, respectively. The dual pumped Er/Ce co-doped fiber amplifier having length $L = 22 \text{ cm}$ exhibited a 28 dB net gain at the wavelength $\lambda = 1558 \text{ nm}$. For the ring laser configuration, the pump laser powers were 316 mW at the wavelength $\lambda = 980 \text{ nm}$ and 141 mW at the wavelength $\lambda = 1480 \text{ nm}$, respectively. A tuning range from 1527 to 1610 nm (83 nm) was achieved.

The recent literature on tellurite glass optimization promises the fabrication of novel optical sources at longer wavelengths and higher efficiencies. As an example, in [20], the Dy-doped tellurite glass samples were used for the time-resolved luminescence spectroscopy measurements. They were prepared from 99.99% high-purity raw materials TeO_2 , ZnF_2 , and Na_2O_3 . The ${}^6\text{H}_{13/2} \rightarrow {}^6\text{H}_{15/2}$ emission band of Dy^{3+} in tellurite glass had a peak at the wavelength close to $\lambda = 2.9 \mu\text{m}$. The peak bandwidth was of about 290 nm and the intrinsic lifetime was about $\tau = 19.6 \mu\text{s}$. Although these results refer to glass sample, the possibility to obtain lasing seems feasible. Moreover, the simulation based on the glass characterization suggested that Dy^{3+} (1 mol.%) -doped tellurite glass may exhibit a population inversion for laser emission at the wavelength $\lambda = 3042 \text{ nm}$.

3. Fluoride Glasses

In addition to tellurite glass, fluoride glass is successfully employed for the fabrication of lasers emitting at long wavelengths. The fluoride glass fiber, made of $\text{ZrF}-\text{BaF}-\text{LaF}-\text{AlF}-\text{NaF}$ (ZBLAN) material, has a relatively low optical absorption in the mid-infrared (IR) spectral region between $\lambda = 1.5 \mu\text{m}$ and $\lambda = 3 \mu\text{m}$. Diode-pumped fluoride glass fiber lasers characterized by different configurations have been recently demonstrated, exhibiting very attractive continuous wave (CW) and pulsed optical power levels at wavelengths close to $\lambda = 2.7 \mu\text{m}$. Fluoride glass fiber lasers can be fabricated at low cost because their set-ups can be based on the employment of commercial laser diodes, which are efficient, reliable and easily available on the market. Therefore, fluoride glasses have been largely employed during the last few decades in order to obtain efficient fiber lasers.

In [21], for the first time, preliminary results on tunable laser emission at wavelengths close to $\lambda_{s1} = 2.31 \mu\text{m}$ in a Tm^{3+} doped monomode fluoride fiber laser were reported. The operation scheme included simultaneous laser action at the wavelength $\lambda_{s2} = 1.82 \mu\text{m}$. The Tm^{3+} ions transitions are

illustrated in Figure 3. CW laser emission over a $\Delta\lambda = 250$ nm tuning range, extending from $\lambda_{s1} = 2.25$ μm to $\lambda_{s1} = 2.5$ μm , was experimented. In particular, a Ti: sapphire laser tuned to the wavelength $\lambda_p = 790$ nm (corresponding to the absorption peak of the ${}^3\text{F}_4$ manifold), acting as pump source, and a monomode ZBLANP fiber having length $L = 10$ m and a refractive index change $\Delta n = 0.007$, were employed. The fiber had a linear polarized LP_{11} mode cutoff at the wavelength $\lambda_{\text{cutoff}} = 2.06$ μm and a low Tm^{3+} doping level, close to $C_{\text{Tm}} = 500$ ppm. The fiber was butt-coupled to a first mirror with reflectivity close to $R_1 = 99.5\%$ in the wavelength range from $\lambda = 2.3$ to $\lambda = 2.7$ μm , and transmission coefficient close to $T_1 = 90\%$ at the pump wavelength. Moreover, a 0.5% output coupler, mirror R_2 , was employed to complete the optical cavity. At the wavelength of $\lambda_{s1} = 2.31$ μm , the threshold pump power for laser oscillation was $P_{\text{th}} = 51$ mW and the maximum observed output power was approximately $P_s = 100$ μW .

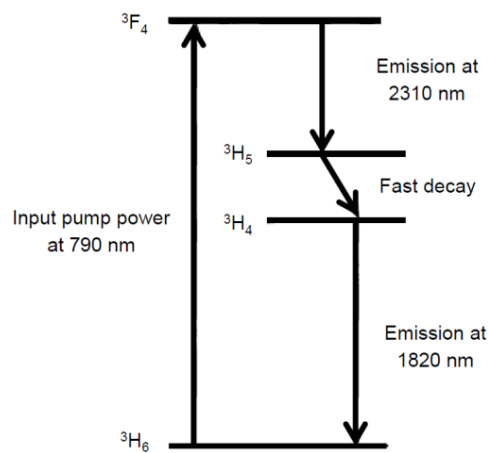


Figure 3. Tm^{3+} doped monomode fluoride fiber laser proposed in [21]. Figure adapted from [21].

In [22], a power-scalable Er^{3+} -doped ZBLAN fiber laser emitting around $\lambda_s = 2.7$ μm , pumped by a tapered amplifier laser diode with an output power of 1 W at 980 nm, was proposed. The CW output power $P_s = 12$ mW was demonstrated. A key factor in the achievement of this relatively efficient performance was the use of high Er concentrations, close to 10,000 ppm, in a fiber with length $L = 5.5$ m. The double-clad fiber had a core diameter $D_c = 6$ μm , a cladding diameter $D_{\text{cl}} = 125$ μm and a numerical aperture $\text{NA} = 0.15$. This result was better than those reported in [23] and [24].

Also, in [25], an Er^{3+} -doped fluoride glass fiber laser was fabricated in order to obtain emission close to the wavelength $\lambda_s = 2.7$ μm , in continuous wave at room temperature. The laser cavity was pumped again with a laser diode at the wavelength $\lambda_p = 980$ nm. The fiber laser was demonstrated in two different fiber output configurations. In the first configuration, a diode laser pump beam was launched into the inner cladding of the fiber via a lens and a dichroic mirror, the other fiber end being closed with a mirror. The second configuration had the diode laser pump beam launched into the inner cladding of the fiber, and the Fresnel reflection was exploited since no mirror was placed at the other fiber end. These configurations are illustrated in Figure 4. The laser characteristics are illustrated in Figure 5. The fiber used for this laser consisted of three coaxial section configurations, with a 35,000 molar ppm ErF_3 , Er-doped, diameter of core of $D_c = 15$ μm and numerical aperture $\text{NA} = 0.16$, inner optical guide region with rectangular shape of 100 $\mu\text{m} \times 200$ μm and numerical aperture $\text{NA} = 0.55$, diameter of outer cladding $D_{\text{cl}} = 300$ μm . A diode pump laser at the wavelength $\lambda = 980$ nm was employed. In particular, the output power versus the pump power for two different lengths are reported. The internal laser diode pump power to fiber optical output power conversion efficiency was $\eta = 27\%$ for the fiber laser having length $L = 8$ m. The laser, suitably focused, produced microholes in paper and chicken fascia tissue. This suggested potential micromachining and microsurgery applications.

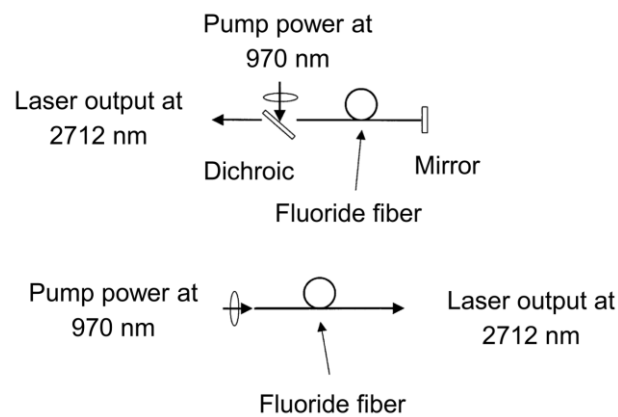


Figure 4. Set-ups of the two fiber laser configurations demonstrated in [25]. Figure adapted from [25].

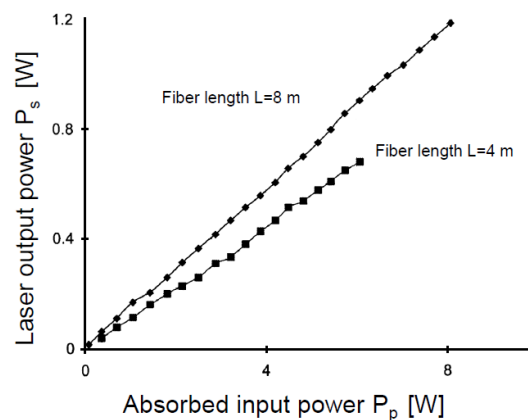


Figure 5. Characteristics of the Er^{3+} -doped fluoride glass fiber laser [25]. Figure adapted from [25].

The ${}^4\text{I}_{11/2} \rightarrow {}^4\text{I}_{13/2}$ transition of erbium ions, at wavelengths close to $\lambda = 2.7\text{--}2.8 \mu\text{m}$, is one of the most used in order to obtain Mid-IR laser emission. This is mainly due to the availability of high power commercial laser diodes at $\lambda = 975 \text{ nm}$, operating in one of the erbium absorption bands. Moreover, the energy transfer upconversion (ETU) process in high concentration erbium doped fibers can be exploited to avoid the drawback caused by the long lifetime of the ${}^4\text{I}_{13/2}$ lower laser level. In [26], the output power $P_s = 8.2 \text{ W}$ at the wavelength of $\lambda_s = 2.8 \mu\text{m}$ from an Er^{3+} -doped fluorozirconate fiber laser was demonstrated. The launched pump power was $P_p = 56 \text{ W}$ at the wavelength $\lambda_p = 975 \text{ nm}$. The optical cavity exploited the cascade lasing with the ground-state transition at $1.6 \mu\text{m}$. In particular, cascade lasing was obtained from simple resonator arrangements, including Fresnel reflection from the ends of the fiber only.

Also, in [27], in order to increase the overall device efficiency, a cascaded erbium doped fluoride fiber laser, based on the two transitions ${}^4\text{I}_{11/2} \rightarrow {}^4\text{I}_{13/2}$ at $\lambda_{s1} = 2.8 \mu\text{m}$ and ${}^4\text{I}_{13/2} \rightarrow {}^4\text{I}_{15/2}$ at $\lambda_{s2} = 1.6 \mu\text{m}$, was fabricated. The cascaded lasing scheme and the pertaining ion transitions are shown in Figure 6. Cascade lasing schemes, such as that of Figure 6, are based on the occurrence that the population inversion exploited for lasing at $\lambda_{s1} = 2.8 \mu\text{m}$ is strengthened by the lasing at $\lambda_{s2} = 1.6 \mu\text{m}$, which depopulates the ${}^4\text{I}_{13/2}$ level. Moreover, the lasing at $\lambda_{s2} = 1.6 \mu\text{m}$ is promoted by the lasing at $\lambda_{s1} = 2.8 \mu\text{m}$, which populates the ${}^4\text{I}_{13/2}$ level.

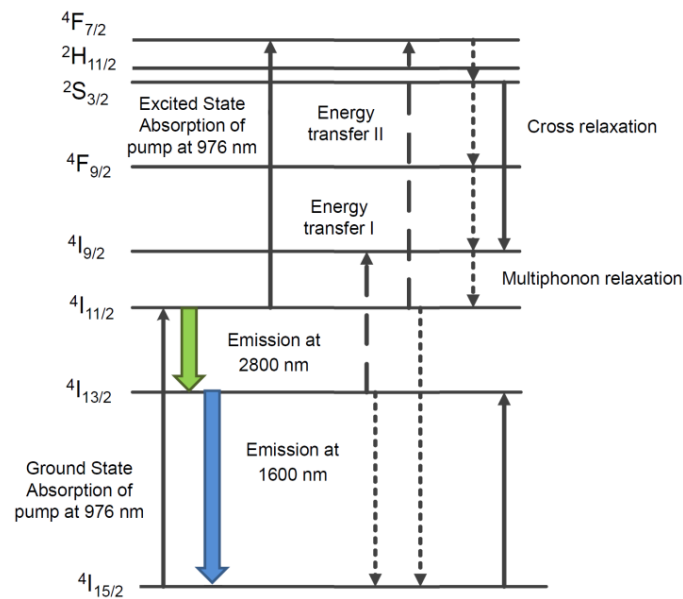


Figure 6. Scheme for the erbium doped fluoride fiber laser based on the cascade of the two transitions $^4I_{11/2} \rightarrow ^4I_{13/2}$ at 2.8 μm and $^4I_{13/2} \rightarrow ^4I_{15/2}$ at 1.6 μm . Figure adapted from [27].

Figure 7 illustrates the characteristics of the fiber laser. The gain fiber was a double-cladding erbium-doped fluoride fiber (FiberLabs., Saitama, Japan) with an octagonal pump core having diameter $D_c = 250 \mu\text{m}$ across the circular cross section, the numerical aperture was $NA = 0.5$, signal core diameter $D_c = 20 \mu\text{m}$, numerical aperture $NA = 0.2$, erbium ions dopant concentration 1.5 mol.%, and fiber length $L = 10 \text{ m}$. In particular, (i) the maximum output power $P_{s1} = 15.2 \text{ W}$ with a slope efficiency $\eta_1 = 26.7\%$ at the wavelength $\lambda_{s1} = 2.8 \mu\text{m}$ and (ii) the maximum output power $P_{s2} = 3.2 \text{ W}$ with a slope efficiency $\eta_2 = 7.1\%$ at the wavelength $\lambda_{s2} = 1.6 \mu\text{m}$ were obtained after the laser optimization. In the aforesaid case, no cooling system was employed. In fact, the overall optical conversion efficiency was very high and the thermal load was low.

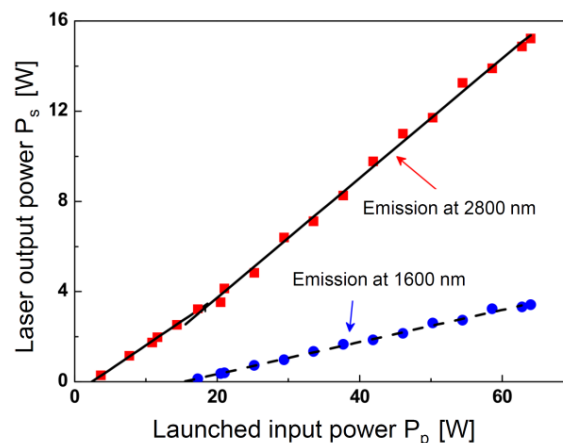


Figure 7. Characteristics of the fluoride fiber laser based on the cascade of the two transitions $^4I_{11/2} \rightarrow ^4I_{13/2}$ at 2.8 μm and $^4I_{13/2} \rightarrow ^4I_{15/2}$ at 1.6 μm . Figure adapted from [27].

In addition to erbium, other dopants have been successfully employed. As an example, in [28], a highly efficient Ho^{3+} -doped fluoride glass fiber laser operating at the wavelength $\lambda_s = 2.08 \mu\text{m}$ was fabricated. A pump laser at the wavelength $\lambda_p = 1.94 \mu\text{m}$ was employed and the maximum slope efficiency $\eta = 78\%$ with an output power $P_s = 516 \text{ mW}$ was obtained.

In [29], a $\text{Ho}^{3+}/\text{Pr}^{3+}$ co-doped fluoride fiber laser with an output power of $P_s = 7.2$ W was demonstrated. It exhibited a slope efficiency of $\eta = 29\%$ and a wavelength tuning range $\Delta\lambda$ between $\lambda = 2825$ nm and $\lambda = 2975$ nm, overlapping with the OH absorption region in many mid-infrared transparent glasses. As pumping system, a diode emission at the wavelength $\lambda_{p1} = 976$ nm was launched into a grating tuned Yb^{3+} fiber laser emitting at $\lambda = 1097$ nm. The Yb^{3+} fiber laser output pumped a Raman laser for $\lambda = 1150$ nm emission, which was coupled into the grating tuned Ho^{3+} , Pr^{3+} co-doped ZBLAN fiber laser.

4. Chalcogenide Glasses

Chalcogenide glass exhibits high rare earth ion solubility. Its high refractive index can increase the emission and absorption cross-sections. It can be drawn into fibers; therefore, this glass is an attractive host material for rare-earth ions. As for the other glasses, different rare earths can be exploited in order to obtain optically active behavior.

Pr^{3+} ions in chalcogenide glass have a high pump absorption cross-section. Moreover, commercially available laser diodes can be employed. Mid-infrared fluorescence from the $(^3\text{F}_2, ^3\text{H}_6) \rightarrow ^3\text{H}_5$ and $^3\text{H}_5 \rightarrow ^3\text{H}_4$ transitions of Pr^{3+} -doped selenide glass have been recently investigated [30–32]. However, a Pr^{3+} -doped selenide chalcogenide glass fiber laser has not yet been constructed for (i) the difficulty of manufacturing high purity rare earth doped chalcogenide glasses and (ii) both the upper and lower laser manifolds have long lifetimes and the population inversion is not easily obtained. Resonant pumping of the Pr^{3+} ions using QCLs was suggested in [30].

In [33], the investigation reported in [30] was extended by considering the ESA processes by using a complete set of experimentally extracted modeling parameters. The laser characteristic, as a function of pump wavelength, fiber length, signal wavelength, fiber background loss and output coupler reflectivity was investigated via a complete model. In particular, the McCumber theory was exploited to extract the ESA absorption cross section spectra. The numerical results showed that ESA strongly affects the laser performance and that its effect can be mitigated by selecting the pump wavelength so that $\sigma_{\text{GSA}} > \sigma_{\text{ESA}}$, via a pumping scheme using a high power QCL. This pumping allows for a strong reduction in the laser threshold and an increase of the laser efficiency.

Dy^{3+} ions in chalcogenide glass have also been extensively investigated [8–11,13,34,35] in order to obtain laser emission in the wavelength range $\Delta\lambda$ between $\lambda = 4.1$ μm and $\lambda = 4.6$ μm by exploiting the $^6\text{H}_{11/2} \rightarrow ^6\text{H}_{13/2}$ transition. However, the long lifetime of the lower laser manifold and the low pump absorption rate are the two major drawbacks limiting the lasing efficiency. In [34], a master oscillator power amplifier (MOPA) configuration, exploiting direct pumping in the upper laser manifold at $\lambda_p = 1.7$ μm , was proposed to reuse the unabsorbed pump power to boost the output signal power by means of an additional amplifying stage. The set-up is shown in Figure 8.

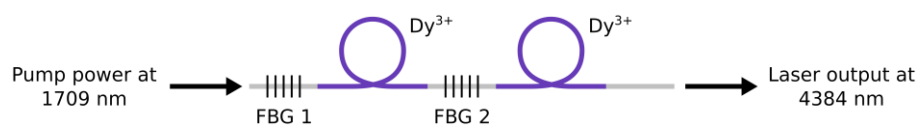


Figure 8. Set-up of the master oscillator power amplifier (MOPA) fiber laser proposed in [34]. Figure adapted from [34].

The simulated optical source was a $\text{Dy}^{3+}:\text{Ga}_5\text{Ge}_{20}\text{Sb}_{10}\text{S}_{65}$ PCF laser, designed to obtain a signal generation close to $\lambda_s = 4400$ nm wavelength. The PCF cross-section allowed single mode propagation at both the pump and signal wavelengths. Three rings of air holes surrounded the rare earth doped solid core. The fiber section geometrical parameters are the hole-to-hole spacing (or pitch) $\Lambda = 8$ μm , hole diameter $d_h = 3.2$ μm , and doped region radius $R_d = 4$ μm . The other geometrical parameters are the laser cavity length $L_1 = 0.3$ m; the fiber amplifier length $L_2 = 1$ m; the first mirror reflectivity $R_1 = 99\%$; and the second mirror reflectivity $R_2 = 70\%$.

The design is performed by considering the measured PCF. Figure 9 illustrates the simulated CW laser characteristics as a function of the Dy^{3+} ions concentration. It can be observed that output powers around $P_s = 550$ mW can be easily obtained with moderately high dopant concentrations, below the glass devitrification limit. An optimized output power $P_s = 637$ mW and an overall efficiency better than $\eta = 21\%$, with an input pump power $P_p = 3$ W, were predicted.

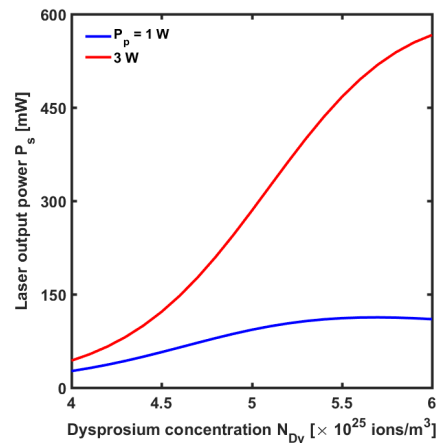


Figure 9. Characteristics of the dysprosium doped chalcogenide fiber laser based on the master oscillator power amplifier (MOPA) configuration. Figure adapted from [34].

In [35], a different approach, based on the employment of QCLs, was adopted. The simulated PCF had the same physical and geometrical parameters. The optical cavity had length $L = 0.5$ m; dopant concentration $N_{\text{Dy}} = 4 \times 10^{25}$ ions/ m^3 ; first mirror reflectivity $R_1 = 99\%$; and second mirror reflectivity $R_2 = 30\%$. A low power optical beam close to the wavelength $\lambda_{p1} = 2.85$ μm was exploited to populate the ${}^6\text{H}_{13/2}$ manifold. This allowed to use a highly efficient in-band pumping at the wavelength $\lambda_{p2} = 4.1$ μm , since the lower laser manifold acted as a virtual ground state. Moreover, the higher absorption cross section of the Dy^{3+} ions for the ${}^6\text{H}_{15/2} \rightarrow {}^6\text{H}_{13/2}$ transition allowed to significantly lower the lasing threshold.

Figure 10 illustrates the simulated characteristics of the fiber laser. By employing an input pump power $P_{p1} = 50$ mW at wavelength $\lambda_{p1} = 2.85$ μm , a slope efficiency as high as $\eta = 38\%$ at the signal wavelength $\lambda_s = 4.38$ μm and a lasing threshold as low as $P_{\text{th}2} = 35$ mW at the pump wavelength $\lambda_{p2} = 4.1$ μm were predicted.

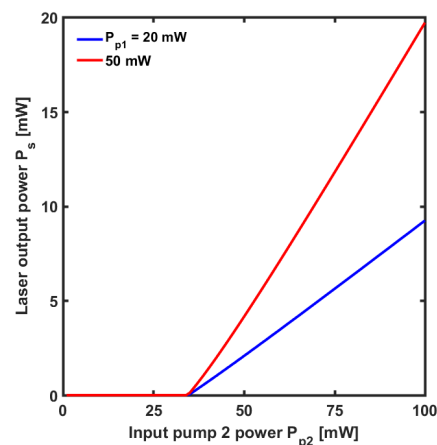


Figure 10. Characteristics of the dysprosium doped chalcogenide fiber laser pumped with quantum cascade lasers (QCLs). Figure adapted from [35].

In [36], mid infrared emission in the 4.3–6.0 μm wavelength range for a Tb^{3+} -doped selenide glass was investigated. A Judd-Ofelt analysis was performed in order to obtain the radiative transition rates. A rate equation approach was exploited to predict the laser performance with respect to pump and signal wavelengths, fiber length, output mirror reflectivity and optical losses. The fiber considered in the simulation had a length $L = 0.1\text{--}3$ m, a core diameter $D_c = 30$ μm , a numerical aperture $\text{NA} = 0.4$ and was doped with 500 ppmw of Tb^{3+} . By employing a pump power of $P_p = 1$ W at the wavelength $\lambda_p = 2.95$ μm , a signal power of about $P_s = 0.4$ W at the wavelength $\lambda_s = 4.7$ μm can be obtained for a fiber loss of 1 dB/m. A slope efficiency better than $\eta = 40\%$ was predicted.

It is also worthwhile to note that rare-earth doped resonant structures, such as microdisks and microspheres, coupled to fibers, could be exploited to obtain narrow line lasing [37,38]. Moreover, different gain media as $\text{Cr}^{3+}:\text{ZnS}$ and $\text{Cr}^{3+}:\text{ZnSe}$ can provide laser emission in the 2–3 μm wavelength range [39].

5. Conclusions

Some recent progresses in Mid-IR fiber lasers are illustrated in this review paper. In some cases, the state of the art includes the feasibility investigation of fabricated Mid-IR fiber lasers, overall for fluoride and tellurite glasses. As an example, for erbium doped fluoride glass fiber laser in cascade configuration, the output power $P_{s1} = 15.2$ W with a slope efficiency $\eta_1 = 26.7\%$ at the wavelength $\lambda_{s1} = 2.8$ μm and the output power $P_{s2} = 3.2$ W with a slope efficiency $\eta_2 = 7.1\%$ at the wavelength $\lambda_{s2} = 1.6$ μm have been measured. In other cases, as for the chalcogenide glasses, the simulation shows great potential but further glass optimizations are required to obtain lasing.

Acknowledgments: This research was partially performed within the COST Action MP1401 Advanced Fibre Laser and Coherent Source as tools for Society, Manufacturing and Lifescience.

Conflicts of Interest: The authors declare no conflict of interest.

References

- Vitiello, M.S.; Scalari, G.; Williams, B.; De Natale, P. Quantum cascade lasers: 20 years of challenges. *Opt. Express* **2015**, *23*, 5167–5182. [[CrossRef](#)] [[PubMed](#)]
- Ebrahim-Zadeh, M.; Kumar, S.C. Yb-Fiber-Laser-Pumped Ultrafast Frequency Conversion Sources from the Mid-Infrared to the Ultraviolet. *IEEE J. Sel. Top. Quantum Electron.* **2014**, *20*, 624–642. [[CrossRef](#)]
- Schliesser, A.; Picqué, N.; Hänsch, T.W. Mid-infrared frequency combs. *Nat. Photonics* **2012**, *6*, 440–449. [[CrossRef](#)]
- Jia, Z.; Wang, L.; Tan, S.; Zhang, J.; Liu, F.; Zhuo, N.; Zhai, S.; Liu, J.; Wang, Z. Improvement of Buried Grating DFB Quantum Cascade Lasers by Small-Angle Tapered Structure. *IEEE Photonics Technol. Lett.* **2017**, *29*, 783–785. [[CrossRef](#)]
- Lin, P.; Li, Y.; Cheng, T.; Suzuki, T.; Ohishi, Y. Coexistence of Photonic Bandgap Guidance and Total Internal Reflection in Photonic Crystal Fiber Based on a High-Index Array With Internal Air Holes. *IEEE J. Sel. Top. Quantum Electron.* **2016**, *22*, 4900606. [[CrossRef](#)]
- Razeghi, M.; Bandyopadhyay, N.; Bai, Y.; Lu, Q.; Slivken, S. Recent advances in mid infrared (3–5 μm) Quantum Cascade Lasers. *Opt. Mater. Express* **2013**, *3*, 1872–1884. [[CrossRef](#)]
- Henderson-Sapir, O.; Jackson, S.D.; Ottaway, D.J. Versatile and widely tunable mid-infrared erbium doped ZBLAN fiber laser. *Opt. Lett.* **2016**, *41*, 1676–1679. [[CrossRef](#)] [[PubMed](#)]
- Seddon, A.B.; Tang, Z.; Furniss, D.; Sujecki, S.; Benson, T.M. Progress in rare-earth-doped mid-infrared fiber lasers. *Opt. Express* **2010**, *18*, 26704–26719. [[CrossRef](#)] [[PubMed](#)]
- Sójka, Ł.; Tang, Z.; Zhu, H.; Bereś-Pawlik, E.; Furniss, D.; Seddon, A.B.; Benson, T.M.; Sujecki, S. Study of mid-infrared laser action in chalcogenide rare earth doped glass with Dy^{3+} , Pr^{3+} and Tb^{3+} . *Opt. Mater. Express* **2012**, *2*, 1632–1640. [[CrossRef](#)]
- Sujecki, S.; Sójka, Ł.; Bereś-Pawlik, E.; Tang, Z.; Furniss, D.; Seddon, A.B.; Benson, T.M. Modelling of a simple Dy^{3+} doped chalcogenide glass fibre laser for mid-infrared light generation. *Opt. Quantum Electron.* **2010**, *42*, 69–79. [[CrossRef](#)]

11. Quimby, R.S.; Shaw, L.B.; Sanghera, J.S.; Aggarwal, I.D. Modeling of Cascade Lasing in Dy: Chalcogenide Glass Fiber Laser with Efficient Output at 4.5 μm . *IEEE Photonics Technol. Lett.* **2008**, *20*, 123–125. [[CrossRef](#)]
12. Hudson, D.D. Short pulse generation in mid-IR fiber lasers. *Opt. Fiber Technol.* **2014**, *20*, 631–641. [[CrossRef](#)]
13. Starecki, F.; Charpentier, F.; Doualan, J.-L.; Quétel, L.; Michel, K.; Chahal, R.; Troles, J.; Bureau, B.; Braud, A.; Camy, P.; et al. Mid-IR optical sensor for CO₂ detection based on fluorescence absorbance of Dy³⁺: Ga₅Ge₂₀Sb₁₀S₆₅ fibers. *Sens. Actuators B* **2015**, *207*, 518–525. [[CrossRef](#)]
14. Ebrahim-Zadeh, M.; Kumar, S.C.; Devi, K. Yb-Fiber-Laser-Pumped Continuous-Wave Frequency Conversion Sources from the Mid-Infrared to the Ultraviolet. *IEEE J. Sel. Topics Quantum Electron.* **2014**, *20*, 350–372. [[CrossRef](#)]
15. Jha, A.; Shen, S.; Naftaly, M. Structural origin of spectral broadening of 1.5- μm emission in Er³⁺-doped tellurite glasses. *Phys. Rev. B* **2000**, *62*, 6215–6227. [[CrossRef](#)]
16. Huang, L.; Shen, S.; Jha, A. Near infrared spectroscopic investigation of Tm³⁺-Yb³⁺ co-doped tellurite glasses. *J. Non-Cryst. Solids* **2004**, *345–346*, 349–353. [[CrossRef](#)]
17. Richards, B.; Tsang, Y.; Binks, D.; Lousteau, J.; Jha, A. Efficient ~2 μm Tm³⁺-doped tellurite fiber laser. *Opt. Lett.* **2008**, *33*, 402–404. [[CrossRef](#)] [[PubMed](#)]
18. Li, L.X.; Wang, W.C.; Zhang, C.F.; Yuan, J.; Zhou, B.; Zhang, Q.Y. 2.0 μm Nd³⁺/Ho³⁺-doped tungsten tellurite fiber laser. *Opt. Mater. Express* **2016**, *6*, 2904–2914. [[CrossRef](#)]
19. Dong, J.; Wei, Y.Q.; Wonfor, A.; Pentyl, R.V.; White, I.H.; Lousteau, J.; Jose, G.; Jha, A. Dual-Pumped Tellurite Fiber Amplifier and Tunable Laser Using Er/Ce Codoping Scheme. *IEEE Photonics Technol. Lett.* **2011**, *23*, 736–738. [[CrossRef](#)]
20. Gomes, L.; Lousteau, J.; Milanese, D.; Mura, E.; Jackson, S.D. Spectroscopy of mid-infrared (2.9 μm) fluorescence and energy transfer in Dy³⁺-doped tellurite glasses. *J. Opt. Soc. Am. B* **2014**, *31*, 429–435. [[CrossRef](#)]
21. Percival, R.M.; Carter, S.F.; Szebesta, D.; Davey, S.T.; Stallard, W.A. Thulium-doped monomode fluoride fibre laser broadly tunable from 2.25 to 2.5 μm . *Electron. Lett.* **1991**, *27*, 1912–1913. [[CrossRef](#)]
22. Poppe, E.; Srinivasan, B.; Jain, R.K. 980 nm diode-pumped continuous wave mid-IR (2.7 μm) fibre laser. *Electron. Lett.* **1998**, *34*, 2331–2333. [[CrossRef](#)]
23. Allen, R.; Esterowitz, L.; Ginther, R.J. Diode-pumped single-mode fluorozirconate fiber laser from the ⁴I_{11/2} → ⁴I_{13/2} transition in erbium. *Appl. Phys. Lett.* **1990**, *56*, 1635–1637. [[CrossRef](#)]
24. Yanagita, H.; Masuda, I.; Yamashita, T.; Toratani, H. Diode laser pumped Er³⁺ fibre laser operation between 2.7–2.8 μm . *Electron. Lett.* **1990**, *26*, 1836–1838. [[CrossRef](#)]
25. Linden, K.J. Fiber Laser with 1.2-W CW Output Power at 2712 nm. *IEEE Photonics Technol. Lett.* **2004**, *16*, 401–403. [[CrossRef](#)]
26. Jackson, S.D.; Pollnau, M.; Li, J. Diode Pumped Erbium Cascade Fiber Lasers. *IEEE J. Quant. Electron.* **2011**, *47*, 471–478. [[CrossRef](#)]
27. Li, J.; Wang, L.; Luo, H.; Xie, J.; Liu, Y. High Power Cascaded Erbium Doped Fluoride Fiber Laser at Room Temperature. *IEEE Photonics Technol. Lett.* **2016**, *28*, 673–676. [[CrossRef](#)]
28. Li, R.; Li, J.; Shterengas, L.; Jackson, S.D. Highly efficient holmium fibre laser diode pumped at 1.94 μm . *Electron. Lett.* **2011**, *47*, 1089–1090. [[CrossRef](#)]
29. Crawford, S.; Hudson, D.D.; Jackson, S.D. High-Power Broadly Tunable 3- μm Fiber Laser for the Measurement of Optical Fiber Loss. *IEEE Photonics J.* **2015**, *7*, 1–9. [[CrossRef](#)]
30. Ferrier, A.; Velázquez, M.; Doualan, J.-L.; Moncorge, R. Spectroscopic investigation and mid-infrared luminescence properties of the Pr³⁺-doped low phonon single crystals CsCdBr₃, KpB₂Cl₅ and Tl₃PbBr₅. *J. Lumin.* **2009**, *129*, 1905–1907. [[CrossRef](#)]
31. Sójka, Ł.; Tang, Z.; Furniss, D.; Sakr, H.; Oladeji, A.; Bereś-Pawlik, E.; Dantanarayana, H.; Faber, E.; Seddon, A.B.; Benson, T.M.; et al. Broadband, mid-infrared emission from Pr³⁺ doped GeAsGaSe chalcogenide fiber, optically clad. *Opt. Mater.* **2014**, *36*, 1076–1082. [[CrossRef](#)]
32. Chahal, R.; Starecki, F.; Boussard-Plédel, C.; Doualan, J.-L.; Michel, K.; Brilland, L.; Braud, A.; Camy, P.; Bureau, B.; Nazabal, V. Fiber evanescent wave spectroscopy based on IR fluorescent chalcogenide fibers. *Sens. Actuators B* **2016**, *229*, 209–216. [[CrossRef](#)]
33. Sójka, Ł.; Tang, Z.; Furniss, D.; Sakr, H.; Bereś-Pawlik, E.; Seddon, A.B.; Benson, T.M.; Sujecki, S. Numerical and experimental investigation of mid-infrared laser action in resonantly pumped Pr³⁺ doped chalcogenide fibre. *Opt. Quantum Electron.* **2017**, *49*, 21. [[CrossRef](#)]

34. Falconi, M.C.; Palma, G.; Starecki, F.; Nazabal, V.; Trolès, J.; Adam, J.-L.; Taccheo, S.; Ferrari, M.; Prudenzano, F. Dysprosium-Doped Chalcogenide Master Oscillator Power Amplifier (MOPA) for Mid-IR Emission. *J. Lightwave Technol.* **2017**, *35*, 265–273. [[CrossRef](#)]
35. Falconi, M.C.; Palma, G.; Starecki, F.; Nazabal, V.; Trolès, J.; Taccheo, S.; Ferrari, M.; Prudenzano, F. Design of an Efficient Pumping Scheme for Mid-IR Dy³⁺:Ga₅Ge₂₀Sb₁₀S₆₅ PCF Fiber Laser. *IEEE Photonics Technol. Lett.* **2016**, *28*, 1984–1987. [[CrossRef](#)]
36. Sojka, L.; Tang, Z.; Furniss, D.; Sakr, H.; Fang, Y.; Beres-Pawlik, E.; Benson, T.M.; Seddon, A.B.; Sujecki, S. Mid-infrared emission in Tb³⁺-doped selenide glass fiber. *J. Opt. Soc. Am. B* **2017**, *34*, A70–A79. [[CrossRef](#)]
37. Palma, G.; Falconi, M.C.; Starecki, F.; Nazabal, V.; Yano, T.; Kishi, T.; Kumagai, T.; Prudenzano, F. Novel double step approach for optical sensing via microsphere WGM resonance. *Opt. Express* **2016**, *24*, 26956–26971. [[CrossRef](#)] [[PubMed](#)]
38. Palma, G.; Falconi, M.C.; Starecki, F.; Nazabal, V.; Ari, J.; Bodiou, L.; Charrier, J.; Dumeige, Y.; Baudet, E.; Prudenzano, F. Design of praseodymium-doped chalcogenide micro-disk emitting at 4.7 μm. *Opt. Express* **2017**, *25*, 7014–7030. [[CrossRef](#)] [[PubMed](#)]
39. Sorokina, I.T.; Sorokin, E. Femtosecond Cr²⁺-Based Lasers. *IEEE J. Sel. Top. Quantum Electron.* **2015**, *21*, 273–291. [[CrossRef](#)]



© 2017 by the authors. Licensee MDPI, Basel, Switzerland. This article is an open access article distributed under the terms and conditions of the Creative Commons Attribution (CC BY) license (<http://creativecommons.org/licenses/by/4.0/>).